

# UC Irvine

## UC Irvine Previously Published Works

### Title

Interactions of gaseous nitric acid with surfaces of environmental interest

### Permalink

<https://escholarship.org/uc/item/6zt1t9sp>

### Journal

Physical Chemistry Chemical Physics, 6(14)

### ISSN

1463-9076 1463-9084

### Authors

Dubowski, Y.  
Sumner, A. L.  
Menke, E. J.  
[et al.](#)

### Publication Date

2004

### DOI

10.1039/b404127e

Peer reviewed

## Interactions of gaseous nitric acid with surfaces of environmental interest

Y. Dubowski,<sup>a</sup> A. L. Sumner,<sup>c</sup> E. J. Menke,<sup>a</sup> D. J. Gaspar,<sup>b</sup> J. T. Newberg,<sup>a</sup>  
R. C. Hoffman,<sup>d</sup> R. M. Penner,<sup>a</sup> J. C. Hemminger<sup>a</sup> and B. J. Finlayson-Pitts\*<sup>a</sup>

<sup>a</sup> Department of Chemistry, University of California Irvine, Irvine CA 92697-2025, USA.

E-mail: [bjfinlay@uci.edu](mailto:bjfinlay@uci.edu); Fax: (949) 824-3168; Tel: (949) 824-7670

<sup>b</sup> Pacific Northwest National Laboratory, P.O. Box 999, MSIN K8-88,  
Richland WA 99352, USA

<sup>c</sup> Now at Battelle, 505 King Ave, Columbus OH 43201-2693

<sup>d</sup> Now at ENVIRON International Corporation, 707 Wilshire Blvd., Suite 4950,  
Los Angeles CA 90017, USA

Received 18th March 2004, Accepted 30th April 2004

First published as an Advance Article on the web 19th May 2004

Gaseous nitric acid removal by surfaces in experimental systems and in the atmospheric boundary layer is rapid. However, neither the form of HNO<sub>3</sub> on surfaces nor its impact on the properties of the thin surface film are known. We report here studies of surfaces that have been exposed at room temperature (295 ± 2 K) to gaseous mixtures of water vapor with HNO<sub>3</sub> at concentrations from 46 ppb to 4 × 10<sup>3</sup> ppm. The surfaces were probed using a combination of Fourier transform infrared spectrometry (FTIR), non-contact atomic force microscopy (AFM), time-of-flight secondary ion mass spectrometry (TOF-SIMS), and X-ray photoelectron spectroscopy (XPS). Exposure of borosilicate glass, quartz, and thin Teflon films to mixtures of gaseous HNO<sub>3</sub> and water vapor leads to the subsequent uptake of much larger amounts of water than occurs on the corresponding unexposed surfaces. Infrared spectra show evidence for the formation of nitric acid–water complexes on the surface that leads to this enhanced water uptake. On borosilicate glass, exposure to the nitric acid–water vapor mixture results in surface segregation of the trace metal oxides and their nitrates formed from reaction with HNO<sub>3</sub>. The majority of these oxides can be removed by rinsing with water; however, smaller, segregated regions of ZnO remain on the surface. The implications for heterogeneous reactions in thin films on surfaces in laboratory systems and in the atmosphere are discussed.

### Introduction

Oxides of nitrogen are ubiquitous in the emissions from fossil fuel combustion and hence are distributed globally.<sup>1</sup> The major NO<sub>x</sub> species emitted, nitric oxide (NO), is eventually oxidized in air to form nitric acid (HNO<sub>3</sub>). Gaseous HNO<sub>3</sub> undergoes both wet and dry deposition onto surfaces in the tropospheric boundary layer, providing a removal mechanism for oxides of nitrogen. These tropospheric surfaces (*e.g.*, aerosols, soils, and urban surfaces such as concrete and glass) also hold thin films of water in which heterogeneous chemistry occurs, including *in situ* formation of HNO<sub>3</sub> via reactions such as the heterogeneous hydrolysis of NO<sub>2</sub>.<sup>2</sup> Although uptake of HNO<sub>3</sub> from the gas phase, or its direct formation on the surface, have historically been assumed to represent the final removal of gaseous oxides of nitrogen from the atmosphere, there is experimental evidence indicating this may not be the case. For example, HNO<sub>3</sub> on surfaces has been shown to react with NO to form gas phase NO<sub>2</sub>.<sup>2–13</sup>

To date, the impacts of deposited HNO<sub>3</sub> on the composition and chemistry of the thin surface films, which potentially have important implications for chemistry in the boundary layer, have not been explored. For example, Diamond *et al.*<sup>14</sup> and Gingrich *et al.*<sup>15</sup> have shown that such surfaces adsorb organics, whose chemistry is expected to be sensitive to the nature and amounts of co-adsorbed species such as HNO<sub>3</sub>, a strong oxidizer.

We report here the results of investigations of the interaction of gaseous nitric acid with surfaces found in the tropospheric

boundary layer and commonly used in laboratory systems: borosilicate glass, quartz, and thin FEP Teflon films. A variety of approaches, including FTIR, atomic force microscopy (AFM), X-ray photoelectron spectroscopy (XPS) and time-of-flight secondary ion mass spectrometry (TOF-SIMS) were utilized. We show that prior exposure of these surfaces to gas phase HNO<sub>3</sub> leads to increased water uptake on the surface. In the case of borosilicate glass, exposure to gaseous HNO<sub>3</sub> leads to segregation of the metal oxides, minor components of the glass, into nitrate-containing “towers”, which may be coated with organics. A nitric acid–water complex was identified by FTIR on the surface during the NO<sub>2</sub> heterogeneous hydrolysis, suggesting that such nitric acid–water complexes may play a role in the increased water uptake. The implications for heterogeneous chemistry in laboratory systems and in the boundary layer are discussed.

### Experimental

#### A. Materials

Three types of surfaces were used to study the effect of HNO<sub>3</sub> on water uptake on surfaces: thin cover slips of smooth borosilicate glass (VWR Microcover glass discs), quartz (Quartz Plus, Inc.) and thin FEP Teflon film (Norton High Performance Films). The cover slips were sufficiently thin that they did not significantly attenuate the infrared beam in the region of interest (above 2000 cm<sup>-1</sup>), allowing measurement of the water bands in the stretching region from 2800 to

4000  $\text{cm}^{-1}$ . The borosilicate glass is composed of 64%  $\text{SiO}_2$ , 9%  $\text{B}_2\text{O}_3$ , 7%  $\text{Na}_2\text{O}$ , 7%  $\text{ZnO}$ , 7%  $\text{K}_2\text{O}$ , 3%  $\text{TiO}_2$  and 3%  $\text{Al}_2\text{O}_3$ . The quartz cover slips were >99.9%  $\text{SiO}_2$  and the Teflon was 0.05 mm FEP (fluoropolymer) Teflon film.

In addition, porous glass was applied to elucidate the infrared absorption spectrum of nitric acid–water complexes using the heterogeneous hydrolysis of  $\text{NO}_2$  as a source of surface  $\text{HNO}_3$ . In these studies, a porous glass disc (Vycor 7930, 14 mm diameter  $\times$  0.24 mm thick, Advanced Glass and Ceramics) was supported in a cell described in detail elsewhere.<sup>16</sup> The disc was moved in and out of the infrared beam to obtain a spectrum of the disc with the gaseous species, and the spectrum of the gases with which the disc was in contact, respectively. The spectrum of surface species was obtained from the difference between these two spectra. Porous glass has a high internal surface area (BET  $\sim$  100  $\text{m}^2 \text{g}^{-1}$ ), and hence is well-suited for obtaining the infrared spectra of small concentrations of surface species.

Aqueous  $\text{HNO}_3$  (Fisher, ACS grade, 69.3 wt.%) was used without further purification, and diluted to the desired concentrations with Nanopure water (18 M $\Omega$  cm). Gaseous nitrogen dioxide was synthesized *via* the reaction of NO (Matheson, CP grade) with  $\text{O}_2$  (Oxygen Services, UHP), and purified as described in detail elsewhere.<sup>2</sup>

## B. Nitric acid exposures

The surfaces of the glass, quartz and Teflon samples were first rinsed with liquid Nanopure water to remove any soluble material<sup>17</sup> and then dried with a flow of  $\text{N}_2$ ; these samples are described throughout as “untreated”. The surfaces were exposed to gaseous nitric acid–water mixtures by placing them in a covered glass container along with an open beaker filled with an aqueous solution of  $\text{HNO}_3$ . The gas phase  $\text{HNO}_3$  concentration was controlled by varying the aqueous concentration of the  $\text{HNO}_3$ . Aqueous phase concentrations of 15.6, 1.5 and 0.55 M gave gas phase  $\text{HNO}_3$  mixing ratios of  $4.3 \times 10^3$  ppm, 0.41 ppm and 46 ppb, respectively, based on the known equilibrium constants.<sup>18–20</sup> The corresponding water vapor partial pressures were 2.9 Torr, 18.5 Torr and 19.3 Torr.<sup>18–20</sup> For simplicity, we refer to the gas phase  $\text{HNO}_3$  concentration throughout, with the understanding that the corresponding water vapor concentration also varies simultaneously. All exposures were carried out at room temperature (295  $\pm$  2 K) under atmospheric pressure with water vapor at equilibrium with the aqueous  $\text{HNO}_3$  solution. The exposure chamber was open to room air prior to covering it during the exposures. Exposure times varied from *ca.* 4 h at the highest  $\text{HNO}_3$  concentration to 11–17 h at the lower concentrations. At the end of each exposure, the sample surfaces were dried for about a minute at room temperature with dry  $\text{N}_2$ . The samples were then placed in the cell used for the water uptake measurements (see below), and were purged with dry  $\text{N}_2$  overnight at *ca.* 313 K to remove volatile  $\text{HNO}_3$  and water from the surfaces.

## C. Water uptake measurements

The amount of liquid water adsorbed on the surfaces was determined as a function of relative humidity (RH) using FTIR as described in detail elsewhere.<sup>17</sup> Briefly, a total of up to 10 cover slips or Teflon pieces were mounted in the cell, allowing for the detection of water uptake on a total of 20 surfaces. Spectra presented here have been normalized to 10 slides (*i.e.*, 20 surfaces) for those cases where fewer slides were used. All gas flows through the cell were set using calibrated flow meters (Matheson TF 1050). The cell and room temperature, maintained at 295  $\pm$  0.2 K, were measured using a type-K thermocouple with an Omega HH202A digital readout unit ( $\pm$ 0.2  $^\circ\text{C}$ ). All measurements were obtained at atmospheric pressure under dynamic conditions with a total flow rate of

200  $\text{mL min}^{-1}$ . Spectra were recorded as interferograms at 1  $\text{cm}^{-1}$  resolution, using 2048 and 1024 scans for background and sample spectra, respectively, on an FTIR spectrometer (Mattson, Galaxy 5020) equipped with a liquid nitrogen cooled mercury cadmium telluride detector.

## D. AFM measurements

Atomic force microscopy (AFM) was used to probe the physical topography of the air/solid interface of the samples described above. Samples were imaged with a vibration-isolated Autoprobe CP atomic force microscope (Park Scientific Instruments (PSI)) under ambient conditions. The images were obtained in non-contact mode with PSI Ultralever C tips. Each 256  $\times$  256 pixel image took *ca.* 10 min to obtain, with a scan rate of 0.5 Hz. Background correction involved the fitting of each scan line in an AFM image with a second order polynomial, and the subtraction of this best fit curve from the raw data. This procedure left intact all surface roughness on a length scale smaller than one-half the image size, but it removed lower frequency noise and the tube curvature artifact from the data. No Fourier filtering of AFM images was carried out.

## E. TOF-SIMS measurements

TOF-SIMS measurements were carried out using a Physical Electronics TRIFT II TOF-SIMS with a  $^{69}\text{Ga}^+$  source in a high mass resolution mode. A pulsed primary ion beam of  $\text{Ga}^+$  ions was directed at the sample surface where the interaction of the primary ions with the sample leads to the ejection of neutral and ionized atoms, molecules, and clusters. The ions were collected and mass separated in a TOF analyzer to obtain a mass spectrum. Two primary ion settings were used in these experiments. In the high mass resolution mode (HMR), a 15 kV, 600 pA (measured with a DC primary beam at the sample) primary pulse was electrostatically bunched, producing a primary pulse width of <1 ns. In the HMR mode under the conditions of this experiment, a mass resolution of *ca.*  $m/\Delta m > 5000$  was achieved, with a focused primary beam of 2–3  $\mu\text{m}$  diameter. In the high spatial resolution (HSR) mode, a 25 kV, 60 pA (measured with a DC primary beam at the sample) primary beam was used to obtain a primary beam diameter of *ca.* 120 nm, at the expense of mass resolution ( $m/\Delta m \sim 1000$ ). Mass specific images or profiles were obtained by defining a mass window to monitor for the entire acquisition (images) or as a function of erosion time (depth profiles).

## F. XPS measurements

X-ray photoelectron spectra of the borosilicate glass and quartz surfaces with and without exposure to  $\text{HNO}_3$  were obtained in an ESCALAB MKII ultra-high vacuum (UHV) instrument (VG Scientific) equipped with three individually pumped chambers, allowing for rapid transfer (<1 h) of samples from atmospheric to UHV pressures. Sample surfaces were irradiated under UHV (*ca.*  $5 \times 10^{-10}$  Torr) with 1486.6 eV X-rays from an aluminum anode at 15 keV and 20 mA. The kinetic energies of the ejected photoelectrons were analyzed using a 150 mm hemispherical electron energy analyzer. Data collection and analysis were carried out using the software package PISCES (Dayta Systems Ltd.). XPS peak areas were integrated after a linear background subtraction. The surface concentrations were determined by dividing the integrated areas by standard sensitivity factors (relative to an F(1s) sensitivity factor of 1.0).<sup>21,22</sup> The sensitivity factors used are as follows: O(1s), 0.721; Si(2p), 0.355; B(1s), 0.165; Zn(2p<sub>3/2</sub>), 3.734; K(2p<sub>3/2</sub>), 1.013; Na(1s), 1.655; Ti(2p<sub>3/2</sub>), 1.360; Al(2p), 0.246. Due to the uncertainty in the sampling depth for each element, the surface composition should be considered semi-quantitative.

## Results and discussion

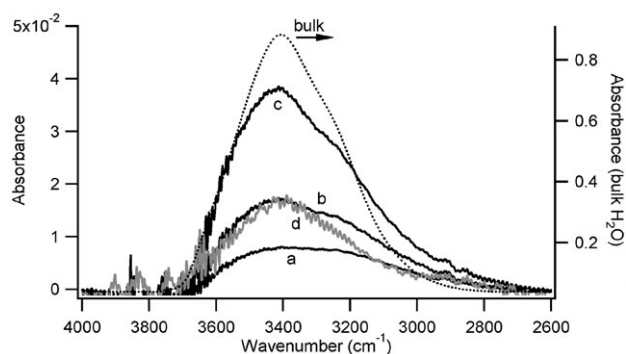
### A. Water uptake

Fig. 1 shows infrared spectra taken at relative humidities from 20 to 79% at 295 K for borosilicate glass cover slips that had been exposed to a mixture of gas phase HNO<sub>3</sub> ( $4 \times 10^3$  ppm) and water vapor (2.9 Torr) for 4 h, followed by purging with dry N<sub>2</sub> at 313 K overnight. After cooling to 295 K, exposure to water vapor was carried out as described in detail elsewhere.<sup>17</sup> It is observed that even at 20% RH, there is significant absorption in the 2800 to 3800 cm<sup>-1</sup> region where the O–H stretching vibrations of bulk liquid water occur, and that this absorption increases with relative humidity. These spectra can be compared to that of bulk liquid water, also shown in Fig. 1. At 20% RH, the peak is broader, suggesting a contribution from another peak at lower wavenumbers than liquid water. Even at the highest RH studied here, there appears to be a small shoulder around 3240 cm<sup>-1</sup>. Also shown in Fig. 1 is a spectrum taken at 80% RH for borosilicate glass without prior exposure to HNO<sub>3</sub> (Fig. 1d). It is clear that the HNO<sub>3</sub>-treated glass (Fig. 1c) has much larger absorptions in this region than the unexposed borosilicate glass. However, the shoulder on the low-wavenumber side of the peaks suggests that the absorption spectra of the HNO<sub>3</sub>-treated glass is not due solely to water. The possibility that the weak absorption of water around 3200 cm<sup>-1</sup>, due to the symmetric OH stretch in a symmetric hydrogen-bonding network,<sup>23</sup> increases upon exposure to HNO<sub>3</sub> seems unlikely, as the presence of HNO<sub>3</sub> on the surface would probably decrease the symmetry of this environment.

Similar results were observed for water uptake on quartz and thin FEP Teflon films exposed to gaseous HNO<sub>3</sub>. For example, Fig. 2a shows infrared spectra for water uptake on HNO<sub>3</sub>-exposed quartz slides, and for comparison, a spectrum for the untreated slides at 80% RH. Fig. 2b shows similar spectra for FEP Teflon film. The shape of the spectra again suggests the presence of a shoulder at ca. 3240 cm<sup>-1</sup>, particularly at the lower relative humidities.

A number of theoretical studies have calculated the vibrational frequencies associated with nitric acid–water complexes.<sup>24–28</sup> Binding of gas phase nitric acid to one water molecule is predicted to red-shift the H–ONO<sub>2</sub> stretch by approximately 400–500 cm<sup>-1</sup> to a ca. 3200 cm<sup>-1</sup> region due to hydrogen bonding between the hydrogen of HNO<sub>3</sub> and the oxygen of water. A similar shift is predicted for HNO<sub>3</sub> hydrogen-bonded to SiH<sub>3</sub>OH or Si(OH)<sub>4</sub>, where hydrogen-bonding to the oxygen of the silica species also occurs.<sup>29</sup> These calculations suggest that the shoulder at ca. 3200 cm<sup>-1</sup> in the spectra (Figs. 1 and 2) is due to a nitric acid–water complex.

In order to elucidate the infrared absorption spectrum of a possible nitric acid–water surface complex, spectra during the



**Fig. 1** Infrared spectra of water uptake on HNO<sub>3</sub>-treated borosilicate glass in contact with N<sub>2</sub> at RH of ca. 20% (a), 50% (b), and 79% (c) (left axis). For comparison, the spectra of bulk liquid water (black dotted line, right axis) and of water uptake on untreated borosilicate glass at 80% RH (gray line, d, left axis) are also shown.

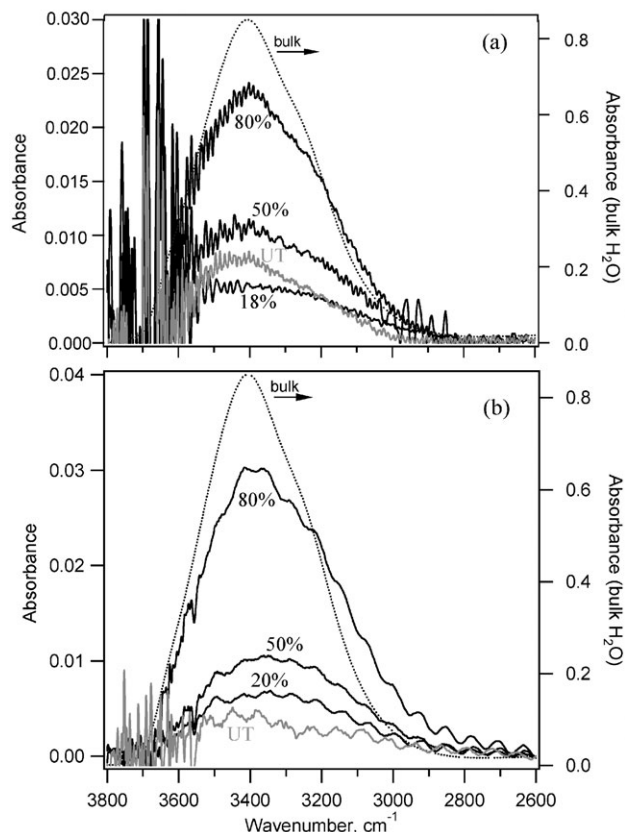


**Fig. 2** Infrared spectra of water uptake on HNO<sub>3</sub>-treated (a) quartz and (b) FEP Teflon film at RH of ca. 20, 50 and 80% in N<sub>2</sub>. For comparison, the spectrum of bulk liquid water (black dashed line) and the spectrum of water on the untreated surfaces at 80% RH are also shown (gray line, UT).

heterogeneous hydrolysis of NO<sub>2</sub> (reaction 1) on porous glass were obtained (Fig. 3).



This approach minimizes the presence of excess HNO<sub>3</sub> relative to water on the surface, avoiding interference with the detection of such complexes due to absorption bands of uncomplexed HNO<sub>3</sub> that are present upon uptake of HNO<sub>3</sub> directly from a gas phase sample. The use of high surface area material such as porous glass provides a much stronger signal for surface species than is possible with geometrically flat surfaces.

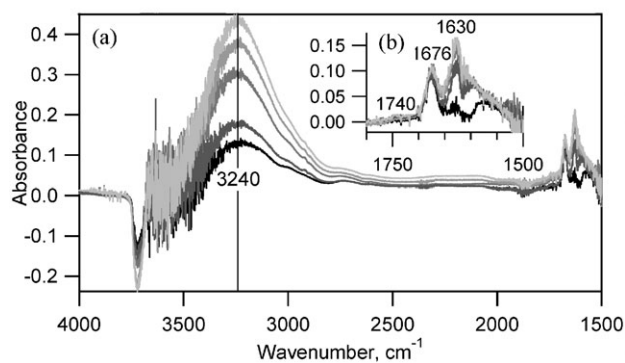


**Fig. 3** (a) Infrared spectra during the room temperature reaction of 0.62 Torr gaseous NO<sub>2</sub> with surface water on porous glass at a total pressure of 746 Torr in N<sub>2</sub> at reaction times of 0, 15, 48, 87, and 106 min (black to light gray, respectively); (b) as in (a) for the 1500–1800 cm<sup>-1</sup> range. Spectra were obtained by ratioing the corresponding single beam spectra to that of the porous glass prior to NO<sub>2</sub> exposure.

The porous glass is hydrophilic and holds water even after brief pumping at room temperature.<sup>30</sup> This surface-adsorbed water provides the reactant for the NO<sub>2</sub> hydrolysis and is available to complex with the nitric acid product as it is formed.

Fig. 3 shows that during NO<sub>2</sub> hydrolysis, a peak in the 3240 cm<sup>-1</sup> region increases (all absorption spectra were obtained by ratioing their corresponding single beam spectra to that of the porous glass prior to exposure to NO<sub>2</sub>). We assign this to a nitric acid–water complex on the surface. Previous theoretical studies<sup>24–29</sup> suggest that this complex may be the 1:1 species, based on the location of the band. However, pending a definitive assignment, we designate this complex as (HNO<sub>3</sub>)<sub>m</sub>(H<sub>2</sub>O)<sub>n</sub>. A peak at 1630 cm<sup>-1</sup> grows in simultaneously, also consistent with a nitric acid–water complex.<sup>24–28</sup> (We could not interrogate this region with the smooth borosilicate glass surfaces due to strong absorption by the substrate below 2000 cm<sup>-1</sup>). The negative band at 3720 cm<sup>-1</sup> is due to binding of the free -SiO-H group to HNO<sub>3</sub>.

The shoulder in Figs. 1 and 2 is therefore likely due to a nitric acid–water complex on the surface. The intensity of the O–H stretch in this complex is predicted to be approximately an order of magnitude larger<sup>24,25</sup> than that in uncomplexed HNO<sub>3</sub> so that even small concentrations of the complex could contribute significantly to the infrared absorption.

The spectra of the HNO<sub>3</sub>-exposed smooth glass and quartz at various relative humidities (Figs. 1 and 2a) were then fit between 2890 and 3660 cm<sup>-1</sup> to a linear combination of the spectra of this nitric acid–water complex and liquid water using a least squares fitting procedure (MFC program),<sup>31</sup> which determines the fraction of each component needed to give a

best fit to the measured spectrum:

$$F(\lambda) = P(\lambda) + \sum_{j=1}^m c_j S_j(\lambda) \quad (1)$$

In eqn. (1),  $F(\lambda)$  is the function that gives the best fit to the measured spectrum,  $P(\lambda)$  is a polynomial that fits the baseline,  $c_j$  is a fit coefficient that is proportional to the true concentration  $C_j$ , and  $S_j(\lambda)$  is the reference spectrum of component  $j$ . In the present case, the reference spectra were taken as bulk liquid water (Fig. 1, dashed line) and the 3240 cm<sup>-1</sup> peak shown in Fig. 3 (106 min) that we have assigned to a nitric acid–water complex. The spectrum of bulk liquid water seems to adequately represent the spectrum of adsorbed water on the treated surfaces, perhaps because water is present on the surface of glass in small islands containing several monolayers (see Fig. 4a and discussion below). Applying the algorithm in eqn. (1) generates the fit coefficients for water and the nitric acid–water complex, which are proportional to the concentrations of these species, as a function of RH.

Fig. 5 shows the fit coefficients thus derived from the measured spectra of HNO<sub>3</sub> exposed borosilicate glass and quartz as a function of RH. On the treated glass, the nitric acid–water complex decreases and the liquid water increases as a function of relative humidity, and at 80% RH, the contribution of the complex to the measured spectrum is small. The significant decrease in the relative amount of the nitric acid–water complex on glass from 50 to 80% RH is consistent with the increasing contribution from adsorbed water, combined with the dissociation of HNO<sub>3</sub> into H<sup>+</sup> and NO<sub>3</sub><sup>-</sup> at higher

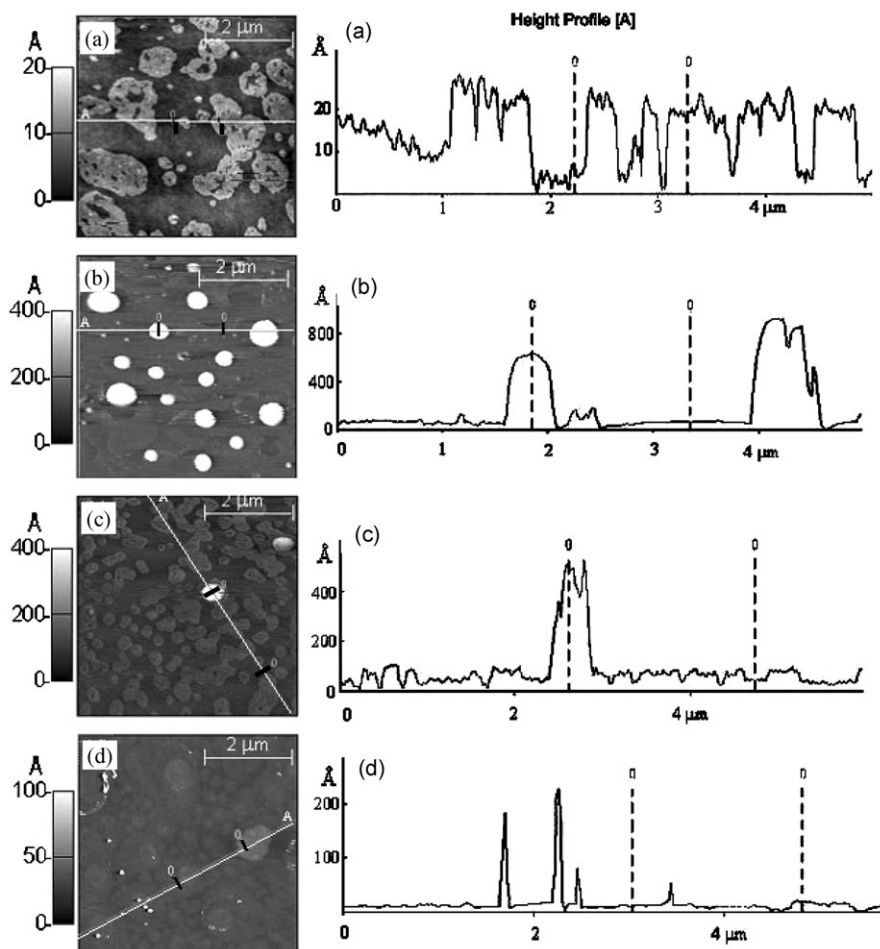


**Fig. 4** AFM images of borosilicate glass (a) untreated; (b) after exposure to  $4 \times 10^3$  ppm HNO<sub>3</sub>; (c) after long exposure to 46 ppb HNO<sub>3</sub>; (d) same as (b) but with a liquid water rinse after exposure. Cross section profiles measured along lines shown on the images are presented on the right (dashed vertical lines correspond to the short black lines on the images).

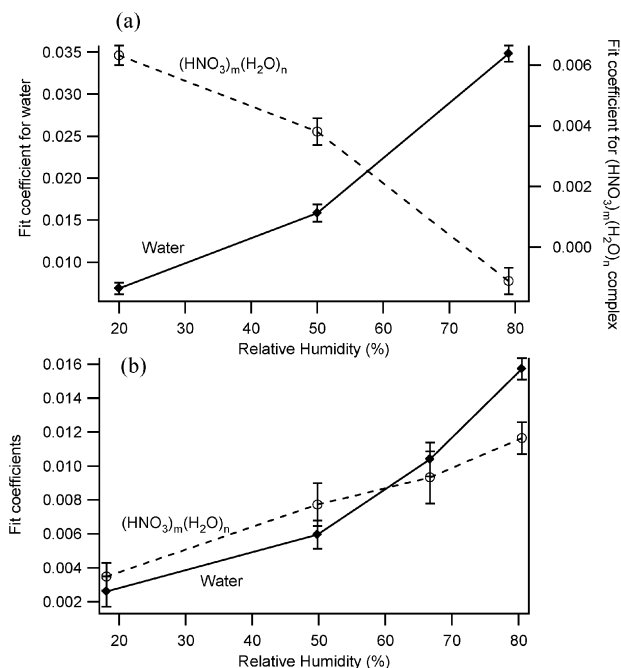


**Fig. 5** Fit coefficients for spectra of liquid water (solid diamonds) and nitric acid–water complex (open circles) in the deconvoluted water uptake spectra on HNO<sub>3</sub> treated (a) borosilicate glass (b) quartz, as a function of RH. Error bars represent only the 1σ for the fit coefficients given by the least squares fitting procedure; the overall error due to the fitting process and subtraction of water vapor bands is expected to be greater.

concentrations of water relative to HNO<sub>3</sub>. For example, in the gas phase, four or more water molecules are required for the ionization of HNO<sub>3</sub>.<sup>32,33</sup> Similarly, the degree of dissociation of HNO<sub>3</sub> in aqueous solutions increases as the solution becomes more dilute.<sup>34,35</sup> As seen in Fig. 6, the amount of water taken up on the treated quartz is significantly smaller than that on treated glass; it is therefore not surprising that the nitric acid–water complex on quartz does not show the same decrease with increasing relative humidity.

While the concentration of the nitric acid–water complex cannot be quantified due to the lack of a reference spectrum at a known concentration, the equivalent number of layers of water on the surface  $\theta$  can be determined using eqn. (2),

$$\theta = \frac{2.303 A_{\text{H}_2\text{O}}}{N S_{\text{H}_2\text{O}} \bar{\sigma}} \quad (2)$$

where  $N$  is the number of surfaces in the infrared beam,  $S_{\text{H}_2\text{O}}$  is the surface density of one water monolayer ( $= 10^{15} \text{ mol cm}^{-2}$ ),  $A_{\text{H}_2\text{O}}$  is the base-10 integrated absorbance of the liquid water

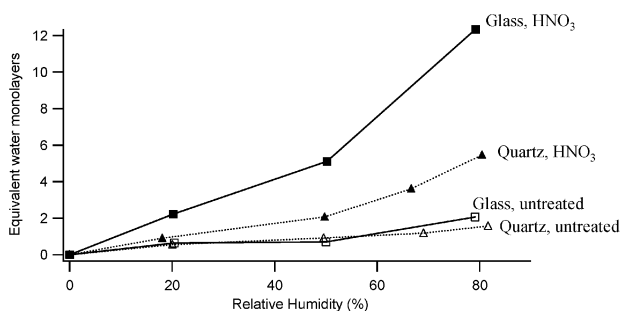


**Fig. 6** Equivalent number of layers of water on borosilicate glass and quartz exposed to  $4 \times 10^3$  ppm HNO<sub>3</sub> (solid squares and solid triangles, respectively), and for comparison, the corresponding data for untreated borosilicate glass (open squares) and quartz (open triangles).

peak (2700–3800  $\text{cm}^{-1}$ ), and  $\bar{\sigma}$  (to base e) is the integrated cross section for liquid water, which was calculated for the same range to be  $1.36 \times 10^{-16} \text{ cm mol}^{-1}$  from optical constants reported by Downing and Williams.<sup>36</sup>  $A_{\text{H}_2\text{O}}$  was calculated from the measured spectrum by determining the portion of the total area that was due to water, using the fit coefficients for water and the HNO<sub>3</sub>·H<sub>2</sub>O complex from the MFC program. The application of this value of  $\bar{\sigma}$  assumes that the absorption cross section of water on the surface is the same as that of bulk liquid water. At relative humidities above ca. 60% at least, this is a reasonable approximation since AFM studies of the height and coverage of water islands on borosilicate glass at the higher RH are in fair agreement with infrared measurements and application of eqn. (2).<sup>17</sup> To acknowledge the uneven distribution of water on the surface, we refer to the water measured using FTIR as an “equivalent number of water layers”.

Fig. 6 shows these calculated equivalent number of water layers on water-rinsed borosilicate glass and on quartz with and without exposure to HNO<sub>3</sub>. Clearly, on both substrates there is a significant increase in the water on the surfaces that had been exposed to HNO<sub>3</sub> compared to the untreated samples. The increase in water uptake is greater for the glass than for the quartz; potential reasons for this are discussed below. Similar quantitative analysis of the spectra for the Teflon was not carried out due to the lack of appropriate reference spectra on Teflon or similar materials; however, the spectra for the Teflon samples (Fig. 2b) clearly also show dramatic increases in water uptake after exposure to HNO<sub>3</sub>.

In short, water uptake on borosilicate glass, FEP Teflon film and quartz surfaces is enhanced by prior exposure to a gaseous nitric acid–water mixture. The presence of a shoulder in the broad absorption peak at ca. 3240  $\text{cm}^{-1}$  is attributed to a nitric acid–water complex, whose concentration on borosilicate glass decreases significantly as the RH increases above 50%.

Bogdan and coworkers<sup>37–39</sup> have reported enhancement of water uptake on silica powders due to HNO<sub>3</sub>. For example, the water film thickness on the powder surface upon exposure to the vapors over a 5–10 wt.% (0.8–1.7 M) aqueous solution of HNO<sub>3</sub> was about twice that upon exposure to water vapor alone,<sup>37</sup> and the mass of water adsorbed from the vapor over a 45 wt.% (9 M) HNO<sub>3</sub> solution per gram of SiO<sub>2</sub> was reported to be about a factor of five larger than the mass adsorbed on exposure to water vapor alone at the same RH.<sup>38</sup> Quartz is primarily silica so that the Bogdan *et al.* results should be comparable to our quartz data; indeed, the data in Fig. 6 show a significant increase in water uptake on quartz at 80% RH. The authors proposed that HNO<sub>3</sub> was adsorbed on the surface, thus changing the nature of the water–silica interaction. This also leads to changes in the freezing and melting temperatures of the thin surface film compared to bulk aqueous HNO<sub>3</sub> solutions, as well as reductions in the enthalpies for freezing and melting.<sup>40</sup> The observed increase in water uptake by silica surfaces upon acid exposure was attributed by the authors to formation of Si-ONO<sub>2</sub> and new silanol groups, reaction (R2),



yielding larger hydrophilic areas on the surface.<sup>38</sup> However, XPS and TOF-SIMS analysis of our smooth glass surfaces (see discussion below) show no significant nitrogen on samples that were rinsed with Nanopure water after exposure to HNO<sub>3</sub>, suggesting that there is not a significant amount of covalently bonded nitrate on the surface. Moreover, in the present study we observe enhanced water uptake upon exposure to gas phase HNO<sub>3</sub> by Teflon films, which do not have silanol groups.

A more likely explanation for water uptake enhancement upon exposure to HNO<sub>3</sub> involves the formation of (HNO<sub>3</sub>)<sub>m</sub>(H<sub>2</sub>O)<sub>n</sub> complexes and the further attraction of water to such complexes. *Ab initio* calculations have shown that the binding energy between a water molecule and HNO<sub>3</sub> is about

twice that between two water molecules, and that addition of water molecules to an existing  $(\text{HNO}_3)_m(\text{H}_2\text{O})_n$  complex is energetically favorable.<sup>26</sup> The presence of adsorbed  $\text{HNO}_3$  on the surface is therefore expected to stimulate water adsorption, forming complexes and water clusters on the surface which further attract water at higher relative humidities.

### B. Effect of nitric acid on surfaces

In order to probe the effect of the nitric acid–water vapor mixture on the surfaces themselves, three different techniques were used: AFM, TOF-SIMS and XPS. AFM was used to examine the borosilicate glass, quartz and Teflon film. XPS analysis was carried out on the borosilicate glass and quartz, and TOF-SIMS on the borosilicate glass. Beam damage prevents the XPS or TOF-SIMS analysis of Teflon.

Fig. 4 shows  $5\ \mu\text{m} \times 5\ \mu\text{m}$  non-contact mode AFM images, measured at *ca.* 60% RH, of water-rinsed borosilicate glass that was (a) otherwise untreated; (b) exposed to the highest concentration ( $4 \times 10^3$  ppm) of  $\text{HNO}_3$ ; (c) exposed to the lowest concentration (46 ppb) of  $\text{HNO}_3$ ; and (d) exposed to the  $\text{HNO}_3$  concentration as in (b) but then rinsed with Nanopure water. On the untreated glass (Fig. 4a), irregular patches can be seen, believed to be islands of water<sup>17</sup> that are  $\leq 2$  nm high. This is the equivalent of *ca.* 3–6 water layers on the surface but as seen in the AFM image, this water is in islands rather than being evenly distributed over the surface. The AFM image in Fig. 4b of the glass that had been exposed to  $\text{HNO}_3$  is quite surprising; large features appear that are

50–90 nm high and *ca.* 0.5–1  $\mu\text{m}$  in diameter. Similar features appear on the glass exposed to the lower concentrations over longer exposure time (Fig. 4c), but are fewer in number. As seen in Fig. 4d, some remnants of these features remained after rinsing with Nanopure water, suggesting that they were largely, but not completely, soluble in water. Both the horizontal size and the height (now *ca.* 20 nm) have been reduced.

On the  $\text{HNO}_3$ -exposed quartz and FEP Teflon films, there were no such unusual surface features. This suggests that these “towers” are not composed of  $\text{HNO}_3$  and water, but rather are associated with the trace elements found in borosilicate glass (B, Zn, K, Na, Ti and Al) and not in the other substrates. To probe the composition of the towers on the borosilicate glass surface, TOF-SIMS analysis was carried out on samples of borosilicate glass that were (i) untreated; (ii) exposed to  $\text{HNO}_3$ ; (iii) rinsed with water after exposure to  $4 \times 10^3$  ppm  $\text{HNO}_3$ . Fig. 7 shows the positive ion images for the surface (a) before and (b) after exposure to  $\text{HNO}_3$  for 4 h. After exposure to  $4 \times 10^3$  ppm  $\text{HNO}_3$ , there are regions with enhanced Zn, K and organics (as indicated by the  $\text{C}_3\text{H}_5$  fragment). These mask the underlying silica so that “holes” appear in the Si image where the Zn and K are found. Sodium is also found in these segregated regions but tends to be more evenly distributed over the surface than Zn and K after the  $\text{HNO}_3$  exposure; this can be seen more readily in the overlay of Na and Si in Fig. 7b where yellow signals indicate the presence of both Na (green) and Si (red). In agreement with the AFM images, similar features were observed after the sample was rinsed with

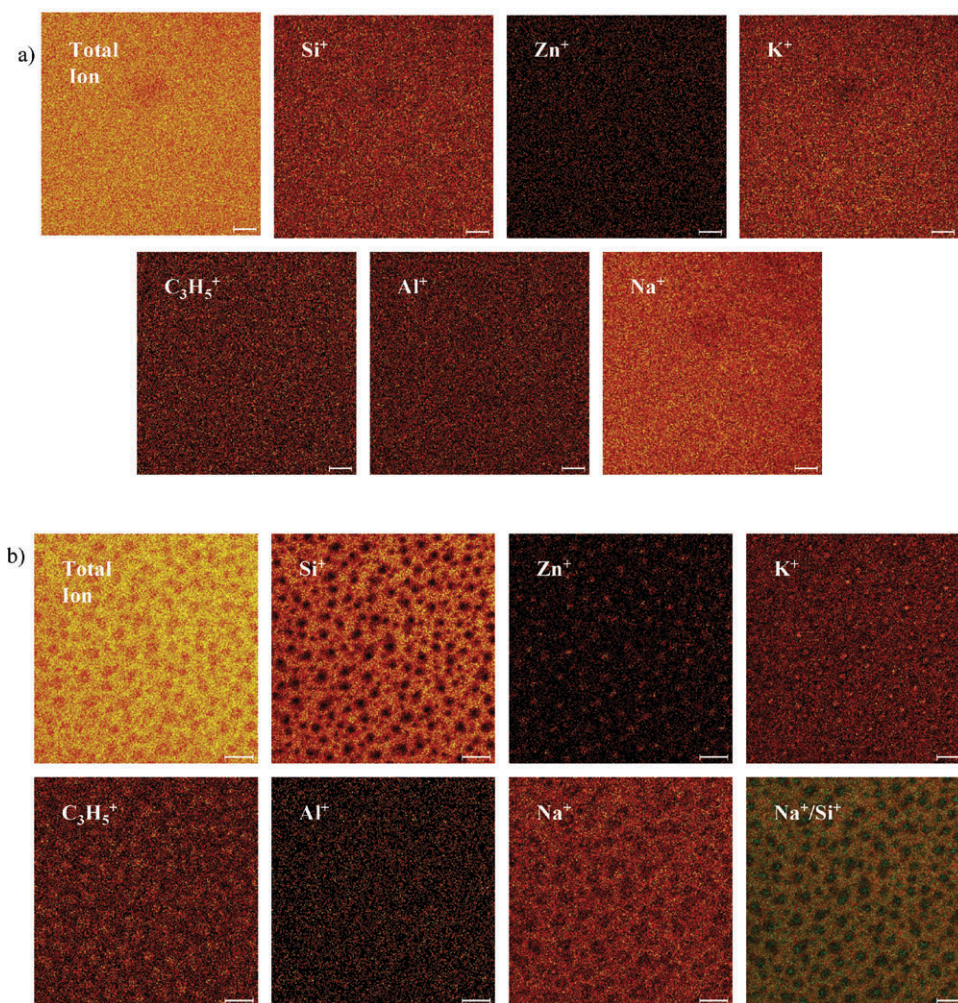


**Fig. 7** TOF-SIMS surface analysis in the positive ion mode for borosilicate glass (a) untreated and (b) after exposure to  $4 \times 10^3$  ppm  $\text{HNO}_3$ . Note: The  $\text{Na}^+/\text{Si}^+$  image shows the individual images of  $\text{Na}^+$  (green) overlaid on the  $\text{Si}^+$  (red) image for clarity. Regions with more yellow are due to the presence of both  $\text{Na}^+$  and  $\text{Si}^+$ . In all TOF-SIMS images, the bars are 10  $\mu\text{m}$  long and lighter colors indicate higher concentrations.

Nanopure water (Fig. 8), but were smaller and less pronounced than before rinsing.

Fig. 9 shows the negative ion images for surface analyses for the H, O, and CH fragments, as well as the total ion signal for both (a) untreated and (b) HNO<sub>3</sub> exposed glass. The regions of elevated H and CH that correspond to “holes” in the O signal (Fig. 9b) suggest that after exposure to  $4 \times 10^3$  ppm HNO<sub>3</sub>, organics are concentrated in regions that appear as “spots” on the surface. Fig. 10 shows a similar analysis but during depth profiling of the sample; these images show the total signals amassed as the sample was probed by the Ga<sup>+</sup> beam down to a depth of *ca.* 3.6 nm. The CH signal decreased after profiling, while these due to oxygen, NO<sub>2</sub>, and NO<sub>3</sub> are more readily apparent. Nitrate is likely present in Fig. 9 but due to its relative low sensitivity, it only becomes apparent when signals are accumulated by depth profiling. Note that due to the complexities of TOF-SIMS ionization processes, this does not imply that these are the actual species on the surface. For example, nitrate ions have a strong NO<sub>2</sub> fragment in TOF-SIMS so that the NO<sub>2</sub> observed here is likely a fragment from nitrate ions. These data are consistent with a surface coating of organics on the segregated regions of metal oxides and metal nitrates, *i.e.*, the relative contribution of the surface organic layer is larger with surface scans.

The TOF-SIMS results show that exposure to gaseous HNO<sub>3</sub> has indeed caused some segregation of trace elements on the surface, as suggested by the AFM images. The “towers” seen by AFM are associated with the trace metals in the borosilicate glass such as Zn, K and some Na. The depth-

profiled images suggest that these include nitrogen, likely in the form of metal nitrates. They may also contain some metal oxides, which are components of the glass before exposure to the HNO<sub>3</sub>. Glass exposed to 0.41 ppm HNO<sub>3</sub> appeared chemically very similar, with somewhat fewer, smaller features. Glass exposed to 46 ppb HNO<sub>3</sub> did not reveal features large enough to be detected *via* TOF-SIMS.

The combination of the AFM and TOF-SIMS data suggest that exposure of the borosilicate glass to the nitric acid–water vapor mixture causes segregation of the Zn, K and some Na on the surface. This is similar to the water-assisted segregation of NaNO<sub>3</sub> on the surface of NaCl after exposure to gas phase HNO<sub>3</sub>.<sup>41–45</sup> In the latter case, hydration of the surface ions increases their mobility and allows them to form stable structures of the product NaNO<sub>3</sub> when the water is removed.

The oxides and hydroxides of Zn, Na and K are expected to react in part with HNO<sub>3</sub> to form the corresponding metal nitrates or the hydrates of the nitrates, all of which are soluble.<sup>46</sup> Unreacted ZnO may also become mobilized on the surface, upon exposure to HNO<sub>3</sub>, as it is soluble in acids.<sup>46</sup> The reduced sizes of the surface features observed by AFM and TOF-SIMS and the removal of the NO<sub>2</sub>/NO<sub>3</sub> signals after rinsing are consistent with the formation of nitrates and their removal by dissolution during rinsing. Sodium and potassium oxides are themselves soluble while ZnO is insoluble in water.<sup>46</sup> Hence rinsing is expected to readily remove the metal nitrates, Na<sub>2</sub>O and K<sub>2</sub>O but to be less efficient in removing the segregated unreacted ZnO due to its lower solubility.

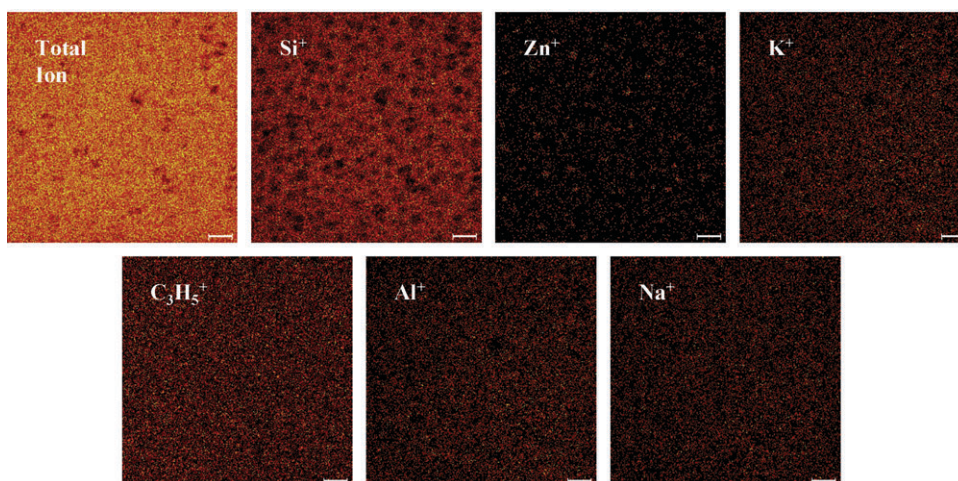


**Fig. 8** TOF-SIMS surface analysis in the positive mode for borosilicate glass exposed to  $4 \times 10^3$  ppm HNO<sub>3</sub>, and then rinsed with liquid water.

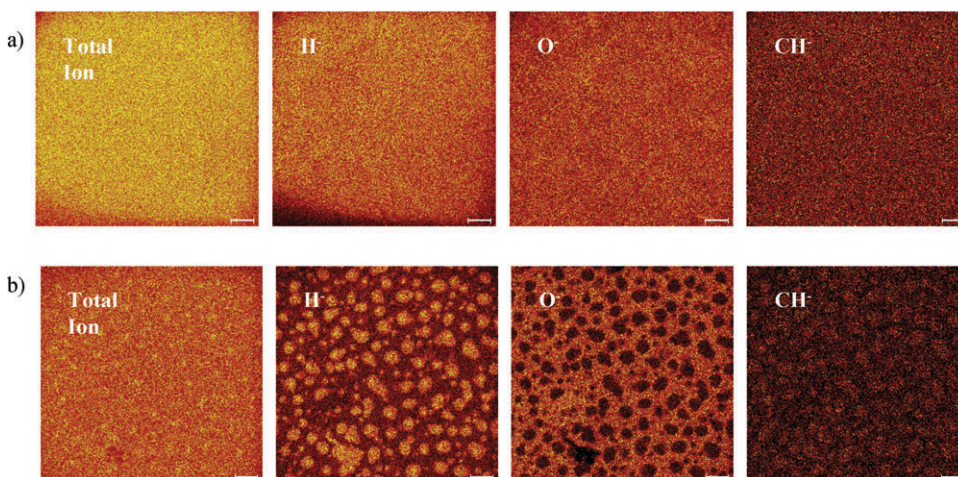


**Fig. 9** TOF-SIMS surface analysis in the negative ion mode for (a) untreated borosilicate glass and (b) after exposure to  $4 \times 10^3$  ppm HNO<sub>3</sub> for 4 h.

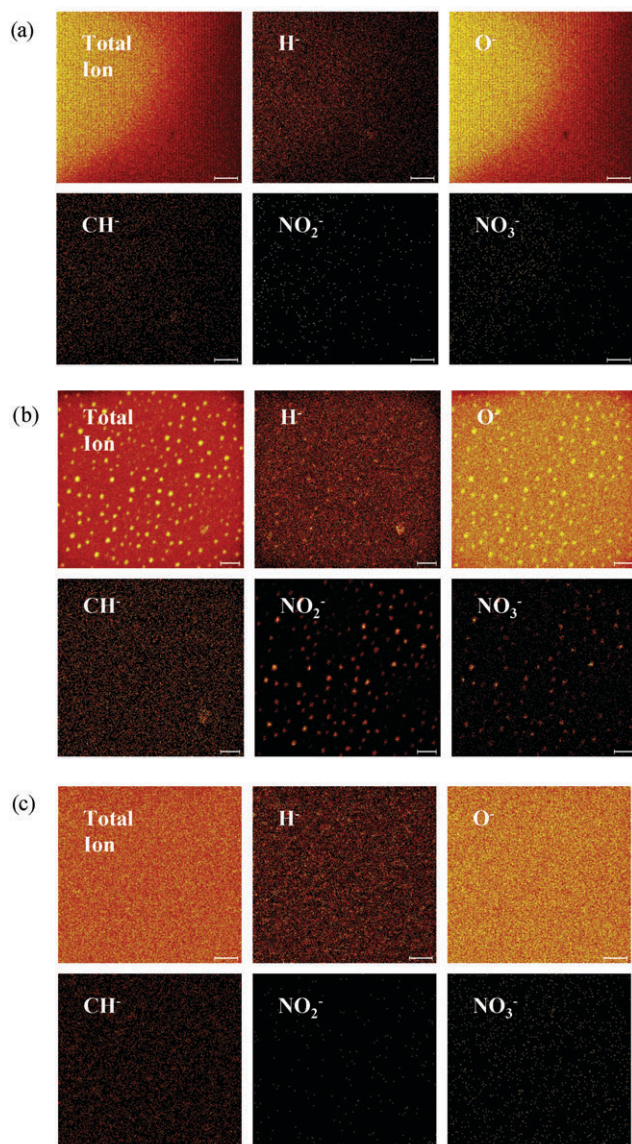


**Fig. 10** TOF-SIMS depth profile analysis in the negative ion mode for borosilicate glass (a) untreated, (b) after exposure to  $4 \times 10^3$  ppm  $\text{HNO}_3$  and (c) same as in sample (b) but rinsed with liquid water after exposure. Asymmetry in untreated glass images is due to incomplete charge compensation.

Consistent with this, features due to zinc segregation are still apparent after rinsing (Fig. 8).

Goodman and coworkers<sup>47</sup> have shown that  $\text{HNO}_3$  dissociates on alumina ( $\text{Al}_2\text{O}_3$ ) and  $\text{TiO}_2$ , which are both insoluble in water and in dilute acids. It is therefore not surprising that Ti and Al do not segregate significantly on the surface upon exposure to gaseous  $\text{HNO}_3$  and water vapor, unlike Zn, K and Na.

This interpretation is consistent with the XPS data shown in Fig. 11. The surface elemental compositions of untreated glass that had been only rinsed with water and the one exposed to  $\text{HNO}_3$ -water vapor show that nitrogen is observed on the  $\text{HNO}_3$  exposed sample, but after rinsing the nitrogen signal is undetectable, as would be expected if they formed soluble nitrates on exposure to  $\text{HNO}_3$ . No increase in nitrogen was observed on quartz surfaces upon exposure to  $\text{HNO}_3$ , consistent with the AFM images that showed no significant change in surface morphology after exposure. These results support our conclusion that metal oxides, which are significant components of borosilicate glass but not of quartz, play a crucial role in the observed surface segregation.

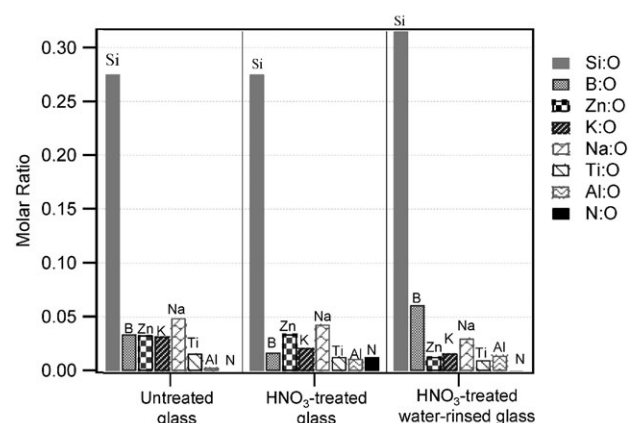


**Fig. 11** XPS analysis of the surfaces of untreated borosilicate glass, borosilicate glass exposed to  $4 \times 10^3$  ppm  $\text{HNO}_3$  for 4 h, and borosilicate glass exposed to  $4 \times 10^3$  ppm  $\text{HNO}_3$  for 4 h and then rinsed with Nanopure water. The molar ratios of various elements relative to oxygen are shown.

As seen in Fig. 6, there is greater water uptake on the treated glass than the treated quartz, despite the fact that the untreated samples adsorb similar amounts of water. Water uptake on surfaces is known to increase with surface roughness, even for hydrophobic materials.<sup>17,48</sup> The enhanced water uptake observed here for glass compared to quartz is attributed to the increased surface roughness of glass caused by the segregation of the trace metal oxides and nitrates on the borosilicate glass. In addition, some of the nitrates, such as  $\text{Zn}(\text{NO}_3)_2$ , are more soluble than their metal oxides and hence would be expected to take up more water as well.

In summary, exposure of both hydrophobic (e.g., FEP Teflon film) and hydrophilic (e.g., borosilicate glass and quartz) surfaces to a gaseous mixture of  $\text{HNO}_3$  and water vapor leads to a surface-adsorbed nitric acid–water complex. These surfaces take up significantly more water from the gas phase than is the case for unexposed surfaces. In the case of borosilicate glass, the  $\text{HNO}_3$  exposure leads to surface segregation of the trace metals, likely as a combination of the metal nitrates and metal oxides. The nitrates and the oxides of sodium and potassium are soluble in water and are removed by rinsing, while some of the zinc oxide, which is far less soluble, remains segregated in towers on the surface.

**Atmospheric implications.** These experiments have important implications for the impact of  $\text{HNO}_3$  on heterogeneous chemistry in the boundary layer and in indoor air environments, as well on building materials. First, the adsorption of  $\text{HNO}_3$  on surfaces, both hydrophobic and hydrophilic, was found to lead to increased water uptake. It is these thin water films on surfaces that control the chemistry on surfaces in the urban and remote boundary layer,<sup>2</sup> and hence the presence of  $\text{HNO}_3$  will play a significant role in determining this chemistry at least in part through its impacts on the amount of adsorbed water. The reactivity of this thin film, which reflects the presence of  $\text{HNO}_3$  and the nature in which it is bound to the surface, remains to be more fully explored.

This study also shows that the  $\text{HNO}_3$  formed by heterogeneous reactions is likely to be adsorbed on the surface in the form of a nitric acid–water complex. Similar complex formation is also expected during other heterogeneous reactions that form  $\text{HNO}_3$ , such as the hydrolysis of  $\text{N}_2\text{O}_5$ .

Finally, these experiments demonstrate that exposure of some building materials and mineral dust particles containing zinc and potassium oxides to  $\text{HNO}_3$  may lead to nitrification of these trace metal components, followed by their dissolution, e.g., by wet deposition. Nitrates have been observed on the

surfaces of building materials, for example in a tunnel in Milan, Italy.<sup>49</sup> From the present results, however, some of the less soluble components such as ZnO can be mobilized and subsequently segregate on the surface. Zinc minerals are found in the Earth's crust (*ca.* 0.02 wt.%) and in the atmosphere.<sup>50</sup> In addition, zinc is widely used in urban areas in paints and die-casting, as a galvanizing agent, and as a component in brass and building materials.<sup>51</sup> Relatively high zinc levels are found in urban and even in indoor fine aerosols.<sup>52</sup> Some fraction of this zinc will be in the form of ZnO, which is a semiconductor with the same band-gap energy as TiO<sub>2</sub> (3.2 eV).<sup>53</sup> Absorption of a photon with energy above the band-gap energy leads to the formation of an electron/hole pair ( $e^-/h^+$ ) in the semiconductor particle. In the presence of suitable scavengers, the recombination of the  $e^-/h^+$  pair is limited, enabling them to react with adsorbed species. Indeed, ZnO is known to act as an efficient photocatalyst for both reduction and oxidation reactions.<sup>53–56</sup> The holes can react with organics to form reactive intermediates or with water to generate OH radicals, and the electron with O<sub>2</sub> to form the superoxide ion, O<sub>2</sub><sup>-</sup>,<sup>57</sup> which reacts with water to generate HO<sub>2</sub> radicals. These reactive intermediates will oxidize organics on the surface which, as seen from the TOF-SIMS data, are associated with the segregated material. Such reactions may play a role in the oxidation of organics observed on some urban surfaces and dust particles.<sup>14,15</sup> In such situations, ZnO may be present in a mixture with other oxides and as very small regions where quantum size effects begin to be important. However, mixtures of metal oxides are also known to have photocatalytic activity, which in some cases is enhanced,<sup>58</sup> and quantum effects in ZnO have not been observed for particles larger than a few nm.<sup>59,60</sup>

In short, it is possible that surface segregation of photocatalysts, such as ZnO, upon exposure to HNO<sub>3</sub>, may contribute to the formation and degradation of important atmospheric species. However, further research is needed to fully understand the role of these semiconductors in such heterogeneous reactions.

## Acknowledgements

We are thankful to the National Science Foundation (grant ATM-0097573) and the Air Resources Board (contract 00-323) for support of this work. A portion of the research described in this paper was performed in the Environmental Molecular Sciences Laboratory, a national scientific user facility sponsored by the Department of Energy's Office of Biological and Environmental Research and located at Pacific Northwest National Laboratory. We thank A. Rivera-Figueroa for the BET surface area measurement of the porous glass. We thank the referees for their efforts and useful comments.

## References

- B. J. Finlayson-Pitts and J. N. Pitts, *Chemistry of the Upper and Lower Atmosphere: Theory, Experiments and Applications*, Academic Press, San Diego, 2000.
- B. J. Finlayson-Pitts, L. M. Wingen, A. L. Sumner, D. Syomin and K. A. Ramazan, *Phys. Chem. Chem. Phys.*, 2003, **5**, 223.
- J. H. Smith, *J. Am. Chem. Soc.*, 1947, **69**, 1741.
- S. Jaffe and H. W. Ford, *J. Phys. Chem.*, 1967, **71**, 1832.
- E. W. Kaiser and C. H. Wu, *J. Phys. Chem.*, 1977, **81**, 1701.
- G. E. Streit, J. S. Wells, F. C. Fehsenfeld and C. J. Howard, *J. Chem. Phys.*, 1979, **70**, 3439.
- I. R. McKinnon, J. G. Mathieson and I. R. Wilson, *J. Phys. Chem.*, 1979, **83**, 779.
- A. C. Besemer and H. Nieboer, *Atmos. Environ.*, 1985, **19**, 507.
- R. Svensson and E. Ljungström, *Int. J. Chem. Kinet.*, 1988, **20**, 857.
- M. Mochida and B. J. Finlayson-Pitts, *J. Phys. Chem. A*, 2000, **104**, 9705.
- N. Saliba, M. Mochida and B. J. Finlayson-Pitts, *Geophys. Res. Lett.*, 2000, **27**, 3229.
- N. Saliba, H. Yang and B. J. Finlayson-Pitts, *J. Phys. Chem. A*, 2001, **105**, 10339.
- A. M. Rivera-Figueroa, A. L. Sumner and B. J. Finlayson-Pitts, *Environ. Sci. Technol.*, 2003, **37**, 548.
- M. L. Diamond, S. E. Gingrich, K. Fertuck, B. E. McCarry, G. A. Stern, B. Billeck, B. Grift, D. Brooker and T. D. Yager, *Environ. Sci. Technol.*, 2000, **34**, 2900.
- S. E. Gingrich, M. L. Diamond, G. A. Stern and B. E. McCarry, *Environ. Sci. Technol.*, 2001, **35**, 4031.
- W. S. Barney and B. J. Finlayson-Pitts, *J. Phys. Chem. A*, 2000, **104**, 171.
- A. L. Sumner, E. J. Menke, Y. Dubowski, J. T. Newberg, R. M. Penner, J. C. Hemminger, L. M. Wingen, T. Brauers and B. J. Finlayson-Pitts, *Phys. Chem. Chem. Phys.*, 2004, **6**, 604.
- K. S. Carslaw, S. L. Clegg and P. Brimblecombe, *J. Phys. Chem.*, 1995, **99**, 11557.
- M. Massucci, S. L. Clegg and P. Brimblecombe, *J. Phys. Chem. A*, 1999, **103**, 4209.
- A. S. Wexler and S. L. Clegg, *J. Geophys. Res.*, 2002, **107**art no. 4207.
- C. S. Hemminger, T. A. Land, A. Christie and J. C. Hemminger, *Surf. Interface Anal.*, 1990, **15**, 323.
- C. D. Wagner, L. E. Davis, M. V. Zeller, J. A. Taylor, R. H. Raymond and L. H. Gale, *Surf. Interface Anal.*, 1981, **3**, 211.
- G. L. Richmond, *Chem. Rev.*, 2002, **102**, 2693.
- F.-M. Tao, K. Higgins, W. Klemperer and D. D. Nelson, *Geophys. Res. Lett.*, 1996, **23**, 1797.
- M. Staikova and D. J. Donaldson, *Phys. Chem. Chem. Phys.*, 2001, **3**, 1999.
- P. R. McCurdy, W. P. Hess and S. S. Xantheas, *J. Phys. Chem. A*, 2002, **106**, 7628.
- R. Escribano, M. Couceiro, P. C. Gómez, E. Carrasco, M. A. Moreno and V. J. Herrero, *J. Phys. Chem. A*, 2003, **107**, 651.
- D. Fernández, V. Botella, V. J. Herrero and R. Escribano, *J. Phys. Chem.*, 2003, **107**, 10608.
- K. C. Thompson and P. Margey, *Phys. Chem. Chem. Phys.*, 2003, **5**, 2970.
- A. V. Kiselev and V. I. Lygin, *Infrared Spectra of Surface Compounds*, Wiley, New York, 1975.
- T. Gomer, T. Brauers, F. Heintz, J. Stutz, U. Platt, University of Heidelberg, 1995.
- B. D. Kay, V. Hermann and A. W. J. Castleman, *Chem. Phys. Lett.*, 1981, **80**, 469.
- J. J. Gilligan and A. W. J. Castleman, *J. Phys. Chem. A*, 2001, **105**, 5601.
- O. Redlich and G. C. Hood, *Discuss. Faraday Soc.*, 1957, **87**.
- E. Högfeldt, *Acta Chem. Scand.*, 1963, **17**, 785.
- H. D. Downing and D. Williams, *J. Geophys. Res.*, 1975, **80**, 1656.
- A. Bogdan, M. Kulmala, B. Gorbunov and A. Kruppa, *J. Colloid Interface Sci.*, 1996, **177**, 79.
- A. Bogdan and M. Kulmala, *J. Colloid Interface Sci.*, 1997, **191**, 95.
- A. Bogdan and M. Kulmala, *Geophys. Res. Lett.*, 1999, **26**, 1433.
- A. Bogdan, M. J. Molina, M. Kulmala, A. R. MacKenzie and A. Laaksonen, *J. Geophys. Res.*, 2003, **108**, AAC1.
- H. C. Allen, J. M. Laux, R. Vogt, B. J. Finlayson-Pitts and J. C. Hemminger, *J. Phys. Chem.*, 1996, **100**, 6371.
- J. M. Laux, T. F. Fister, B. J. Finlayson-Pitts and J. C. Hemminger, *J. Phys. Chem.*, 1996, **100**, 19891.
- S. Ghosal and J. C. Hemminger, *J. Phys. Chem. A*, 1999, **103**, 4777.
- B. J. Finlayson-Pitts and J. C. Hemminger, *J. Phys. Chem. A*, 2000, **104**, 11463.
- J. C. Hemminger, *Int. Rev. Phys. Chem.*, 1999, **18**, 387.
- D. R. Lide, *Handbook of Chemistry and Physics*, CRC Press, Boca Raton, FL, 2001/2002, vol. 82.
- A. L. Goodman, E. T. Bernard and V. Grassian, *J. Phys. Chem. A*, 2001, **105**, 6443.
- Y. Rudich, I. Benjamin, R. Naaman, E. Thomas, S. Trakhtenberg and R. Ussyshkin, *J. Phys. Chem. A*, 2000, **104**, 5238.
- N. Marinoni, M. P. Birelli, C. Rostagno and A. Pavese, *Atmos. Environ.*, 2003, **37**, 4701.
- L. Schutz and K. A. Rahn, *Atmos. Environ.*, 1982, **16**, 171.
- M. Co, *Merck Index*, Rathway, NJ, 9th edn., 1976.
- C. Y. Chao and K. K. Wong, *Atmos. Environ.*, 2002, **36**, 265.
- J. Villasenor and H. D. Mansilla, *J. Photochem. Photobiol., A: Chem.*, 1996, **93**, 205.

- 54 C. Kormann, D. W. Bahnemann and M. R. Hoffmann, *Environ. Sci. Technol.*, 1988, **22**, 798.
- 55 M. Shimokawabe, A. Ohi and N. Takezawa, *React. Kinet. Catal. Lett.*, 1994, **52**, 393.
- 56 B. Pal and M. Sharon, *Mater. Chem. Phys.*, 2002, **76**, 82.
- 57 M. Kaneko and I. Okura, *Photocatalysis: Science and Technology*, Kodansha Springer-Verlag: Tokyo, 2002.
- 58 Z. H. Yuan, J. H. Jia and L. D. Zhang, *Mater. Chem. Phys.*, 2002, **73**, 323.
- 59 R. M. Nyffenegger, B. Craft, M. Shaaban, S. Gorer, G. Erley and R. M. Penner, *Chem. Mater.*, 1998, **10**, 1120.
- 60 R. Viswanatha, S. Sapra, B. Satpati, P. V. Satyam, B. N. Dev and D. D. Sarma, *J. Mater. Chem.*, 2004, **14**, 661.